

See discussions, stats, and author profiles for this publication at: <https://www.researchgate.net/publication/348011486>

Dimensional metrology of additively manufactured lattice structures by combined tactile probe and X-ray tomography

Article in *Material Design & Processing Communications* · December 2020

DOI: 10.1002/mdp.2.216

CITATIONS

0

READS

30

5 authors, including:



Anton Du Plessis

Stellenbosch University

227 PUBLICATIONS 1,667 CITATIONS

[SEE PROFILE](#)



Marco Zago

Università degli Studi di Trento

6 PUBLICATIONS 11 CITATIONS

[SEE PROFILE](#)

Some of the authors of this publication are also working on these related projects:



Improving postharvest preservation sheet quality [View project](#)



Lattice structures [View project](#)

Dimensional metrology of additively manufactured lattice structures by combined tactile probe and X-ray tomography

Anton du Plessis^{1,2}  | Gerd Schwaderer³ | Ilaria Cristofolini⁴ | Marco Zago⁴ | Matteo Benedetti⁴ 

¹Research Group 3D Innovation, Stellenbosch University, Stellenbosch, South Africa

²Department of Mechanical Engineering, Nelson Mandela University, Port Elizabeth, South Africa

³Volume Graphics GmbH, Heidelberg, Germany

⁴Department of Industrial Engineering, University of Trento, Trento, Italy

Correspondence

Anton du Plessis, Research Group 3D Innovation, Stellenbosch University, Stellenbosch 7602, South Africa.
Email: anton2@sun.ac.za

Abstract

Additive manufacturing allows high complexity of manufactured structures, permitting entirely new design capabilities. In the context of complex design, lattice structures hold the most promise for high complexity, tailorable and ultra-lightweight structures. These unique structures are suitable for various applications including light-weighting, energy absorption, vibration isolation, thermal management amongst many others. This new complexity leads to new manufacturing quality control and metrology challenges. Traditional metrology tools cannot access the entire structure, and the only reliable method to inspect the inner details of these structures is by X-ray computed tomography (CT). This work highlights the challenges of this process, demonstrating a novel workflow for dimensional metrology of coupon lattice samples—using a combination of surface and internal metrology using tactile probe and CT. This dual combined approach uses traditional surface coordinate measurement on exterior accessible surfaces, which is followed by internal lattice measurements. The results show a clear method and workflow for combining these technologies for a holistic dimensional inspection. The confidence gained by inspection of such lattice coupons will support the application of these lattices in end-use parts.

KEYWORDS

calibration, laser powder bed fusion, lattice structures, metal additive manufacturing, metrology, X-ray tomography

1 | INTRODUCTION

Additive manufacturing (AM) has grown significantly in recent years with increasing industrial applications.¹ Additive manufacturing processes allow a new level of manufacturing complexity and design possibilities not previously possible.^{2,3} Although all forms of AM show promise for industrial applications, metal AM and in particular laser powder bed fusion (L-PBF) has already been adopted in some critical applications in medical and aerospace applications due to their reliability and excellent properties.^{4–6} Further adoption of this technology depends mainly on the potential advantages gained, of which complexity of design is a major driver. In complex design, cellular lattice structures in particular are very promising. The repetitive arrangement of space-filling unit cells acts similar to an open cell foam^{7,8} but with the advantage that they may be designed and tuned more precisely to fit the application.⁹ In the medical industry, additively manufactured lattice structures find application in bone implants where their porous nature allows bone

ingrowth and better matching of the effective elastic modulus of the porous metallic structure to that of bone, limiting stress shielding effects.^{10,11} In automotive and aerospace industries, they hold great promise for load bearing structural applications with extreme light-weighting capabilities. Reviews of lattice structures fabricated by additive manufacturing, discussing these and more applications are found in previous studies.^{9,12–14} Despite these advantages and potential, the measurement and validation of manufacturing quality of such complex structures is a challenge. Computed tomography (CT) is useful in this regard, for inspection of internal details of complex structures such as lattice structures.¹⁵ An example of the need for internal measurements in such structures is shown in Figure 1, where a lattice has some major build errors internal to the lattice as indicated, compared with the computer-aided design (CAD) design (yellow). These errors are not visible from the surface and only detectable by CT. This an extreme example of manufacturing error causing mismatch between the CAD geometry and as-built part geometry. Various causes exist for these mismatches, including the combination of process parameters and scan strategy, relative to the feature sizes, the angle and length of the strut, orientation relative to the build direction, the surface roughness, amongst others. The fundamentals of the laser powder bed fusion process, which explain the different possible mechanisms for geometrical inaccuracies, as well as the effects of post-processing on the accuracy of parts, are described in more detail in previous studies.^{4,16–18}

Dimensional metrology tools such as coordinate measurement machines (CMMs) operate on the principle of touch-probe contact measurements at extremely high accuracy with high precision and traceability of measurements. The process is manual and involves measuring selected points on the surface of the part or in shallow accessible features, as decided beforehand according to predefined acceptance/testing criteria. The use of metrology for inspection and validation of parts in the manufacturing industry is well developed and holds clear economic benefits as described in Savio et al.¹⁹ It is especially useful for checking tolerances of critical components and for first-article inspection, to ensure a quality manufacturing process. It is, however, only limited to surface measurements that are accessible by the CMM probe.

In the industrial metrology domain, X-ray CT has over the years increased in its capabilities, specifically with metrology-grade CT systems available in recent years. The development of CT in relation to metrology is described in previous studies.^{20–23} In particular, it is useful to highlight a study showing CMM and CT measurements in direct comparison and discussing the relative measurement uncertainty, in most cases only 5 μm .²⁴ The main advantage of CT is the ability to measure internal features nondestructively, which is not possible using CMM. The additional advantages of CT applied to AM are the possibilities of evaluating internal porosity or other defects, assessing surface quality, estimating part conformance to the design and enabling finite element structural analyses of the actual geometry of intricate cellular lattice materials.^{25–30} Metrology CT systems have been demonstrated to be accurate to better than 2 μm in a study using a test artefact for direct comparison between CMM and CT.³¹ Test artefacts have been developed in various groups for improved dimensional measurement traceability and for calibrating CT systems.^{32,33} Metrology CT of lattice structures was recently reported in Zanini et al.,³⁴ where the uncertainty was investigated in metrological measurements using different approaches, for these complex structures.

However, metrology CT systems are not yet as widely available as typical industrial CT systems, different materials may cause differences in CT results, and scans can be done in different ways affecting the results.³⁵ This results in the traceability and measurement accuracy of typical CT dimensional measurements often being a concern.

In this work, we demonstrate a relatively simple and synergistic solution by combining highly accurate external-surface metrology by CMM and internal metrology by industrial CT on the same complex test object. The object is not

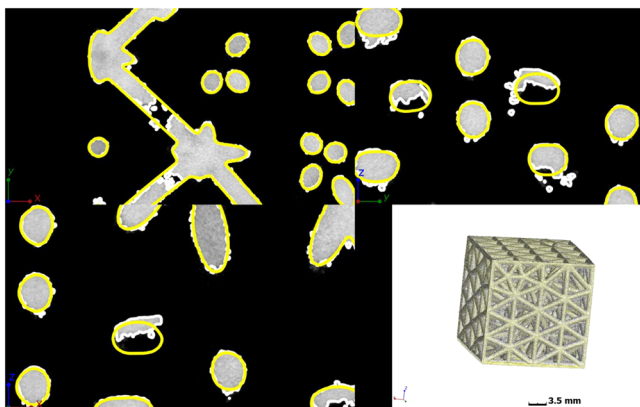


FIGURE 1 Example of internal struts of a lattice with serious manufacturing error, shown in three orthogonal cross-sectional views from computed tomography (CT) data, compared to computer-aided design (CAD) geometry (yellow)

an artefact but rather a lattice structure: an example of a complex structure manufactured by additive manufacturing. This means that the actual object is measured in two methods. In this dual combined approach, a CMM is used to measure the same points in recorded CT data, allowing direct comparison, and in principle, a virtual calibration of the CT dataset is possible. This methodology is relevant for complex parts requiring internal measurements with CMM traceability. This case study demonstrates the capability for two lattice styles—strut-based and gyroid designs. This highlights some interesting and important challenges and provides guidelines for metrology of such complex additively manufactured parts.

2 | METHODS

Two lattice designs were used in this work—the strut (or beam) based version (Figure 2, left) is nonsymmetric due to its design by simulation using Altair Inspire software. The design process involves selection of target design volume, material fraction, stiffness and minimal and maximal strut thickness constraints. In this case, the design was performed with a 25% total density target (material fraction). A gyroid lattice was designed to match the strut based version with the same total density and similar effective strut thickness (Figure 2, right). The gyroid is a skeletal-style minimal surface design, with some advantages in that its manufacturing is self-supporting and lacks stress concentrations such as found at nodes in the strut-based lattices. The samples were manufactured in Ti6Al4V (ELI) using an EOS M290 laser powder bed fusion system, with optimal (prescribed) process parameters for this material. Similar work was reported recently in du Plessis et al.,³⁶ using the same process and materials.

The CMM measurements were performed by a Hexagon DEA Global Image 07-07-07 coordinate measuring machine equipped with a Renishaw SP600M touch-probe with an accuracy of $1.5 + L/333 \mu\text{m}$ and the resolution of $0.08 \mu\text{m}$ in point by point measurement according to ISO 10360-2.³⁷

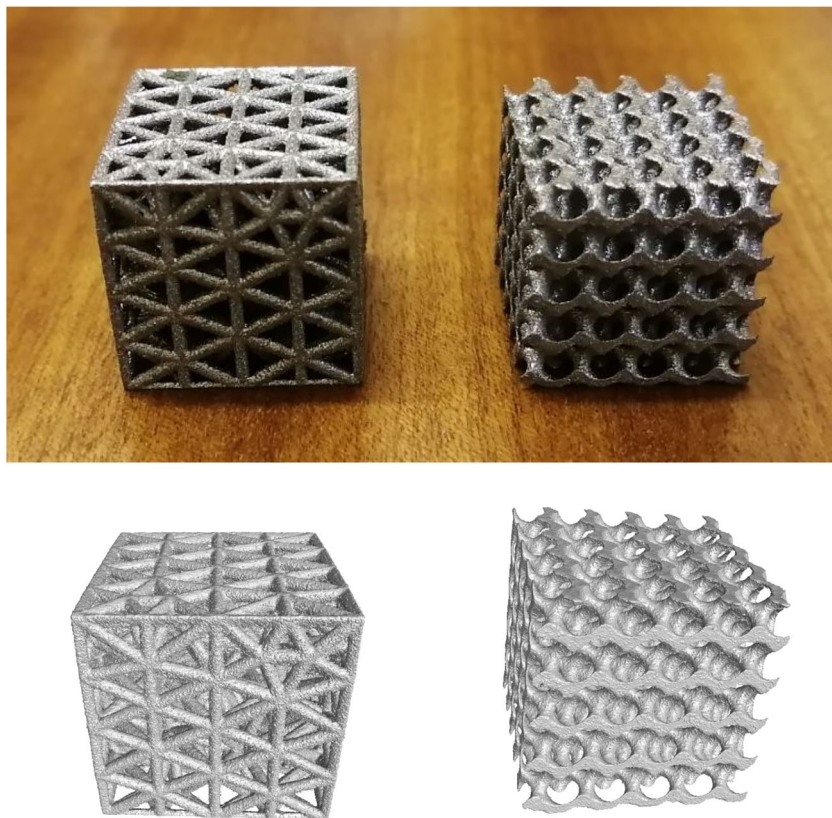


FIGURE 2 Two lattice structure samples used in this study shown in photo (top) and computed tomography (CT) rendering (bottom), the total width of each is 20 mm, density is 25% (material fraction). The simulation-optimized strut-based design is shown to the left and the gyroid design to the right

The probe mounted a stylus having an effective working length of 20.5 mm and a tip sphere of 1 mm, aiming at both inspecting the very small features in the samples and avoiding any collision with the clamping system and the support frame. Figure 3 displays the clamping system adopted for the strut-based design. The strut-based lattice was aligned by a 3,2,1 alignment method, the primary datum plane was identified on the upper surface perpendicular to the build direction (Z), the secondary and tertiary datum planes were identified on the planes perpendicular to the X and Y CAD directions, respectively.

Eight to 10 points were acquired on each surface of strut-based lattice. Because the surfaces are not flat (due to inherent surface roughness), the points were carefully selected in order to touch the junction of struts, as shown in Figure 3. The points at strut junctions are theoretically more reliable, because the contact area should be practically unaffected by the curvature of the converging cylindrical struts. A Gaussian best-fit least squares method was implemented to derive the planes from the measured points. The distance between opposite planes permits to estimate the dimensions of the lattice; this value is given by the distance of the centroids of the theoretically parallel opposite planes projected into the related working plane. For sake of clarity, let us consider the dimension of the strut-based lattice along the Y direction. The centroids of planes parallel to the XZ plane are projected into the YZ plane (working plane X) and the distance between the planes are calculated by the difference of Y coordinates of the centroids.

Because this measurement procedure could be virtually impaired by the absence of actual plane surfaces on the sample, an alternative (second) approach was developed for assessing the lattice dimensions. According to sample design, on each opposite face, there is a cylindrical strut in the middle of the face, as illustrated in Figure 4. Therefore, the distance between the cylinders' axes can also provide the sample dimension: despite the small angular sector measurable on each cylinder, from 15 to 20 points were acquired. Points were carefully selected in order to avoid any contact with the inclined strut, which could have a detrimental effect on the measurement. A Gaussian best fit least squares method was adopted for the cylinder reconstruction. After the measurement of the opposite cylinders, the

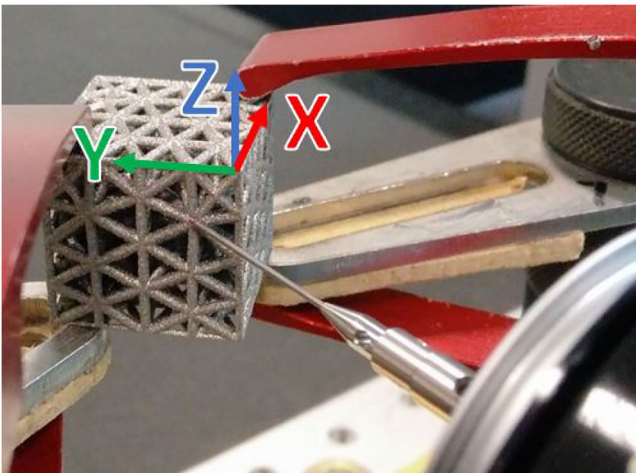


FIGURE 3 Clamping configuration of strut-based sample on the coordinate measurement machine (CMM) working plane, 3D reference system identified on the sample and an example of the touching point at the junction of strut

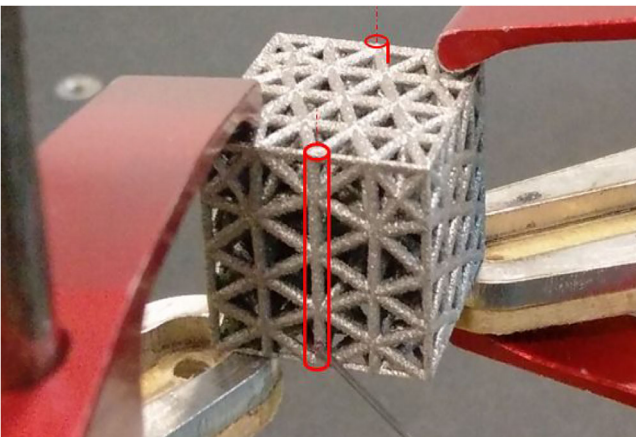


FIGURE 4 Example of opposite cylinders used for evaluating the actual dimensions of the strut-based lattice samples

distance was calculated by the distance between the centroids of the cylinders, according to the procedure previously described for opposite planes.

A similar measurement procedure was adopted for the gyroid sample. Figure 5 shows the clamping configuration, which allows the optimum access to all the surfaces. A 3,2,1 alignment procedure was utilized. The primary datum plane was identified on the bottom surface perpendicular to the printing direction (the surface derived from cutting the part from the building plate), as shown in Figure 6. The secondary and tertiary datum planes were identified by the planes perpendicular to X and Y CAD directions, respectively.

Twenty points minimum were acquired on each surface, in order to reconstruct the planes by a Gaussian best fit least squares method. The distance between planes was then evaluated by the same approach used on the strut-based lattice. On this sample, the measurement was repeated several times changing the probe orientation and rotating the sample in the clamping system. The analysis of the data did not reveal an appreciable influence of probe orientation, as expected. On the other hand, an improper position of the sample and less careful manual alignment might create a moderate discrepancy of CMM measurement, due to lack of correspondence between the measured points and their nominal inspection position.

X-ray micro CT was performed at the Stellenbosch CT facility.³⁸ The scans were performed with 200 kV, 100 μ A at 25 μ m voxel size. A subvoxel interpolation was used for the thresholding process to find the accurate edge of the material (called an advanced surface determination, using a 4-voxel local thresholding search distance at all points along the interface between air and material), and this was used for further CT metrology measurements. The CT metrology measurements were done using VG Studio Max standard metrology functionality for fitting Geometry Elements, alignment, creation of coordinate systems and dimensional metrology. The measurement process for each design is discussed separately below.

Initially, the measurements were taken without considering the ability of a CMM to measure in a similar way as one can do in CT data, simply selecting any maximum point on specific surfaces. So, to make the measurements more comparable, and mimic the alignment used with the CMM, it is more suitable to adapt CT to CMM, although a lot of the advantages using an almost indefinite number of measurement points somewhat gets lost in this process. As a brief explanation, the points probed with a CMM can be used in the CT measurement by using the same XYZ coordinate



FIGURE 5 Clamping configuration of lattice gyroid sample in the coordinate measurement machine (CMM) working plane

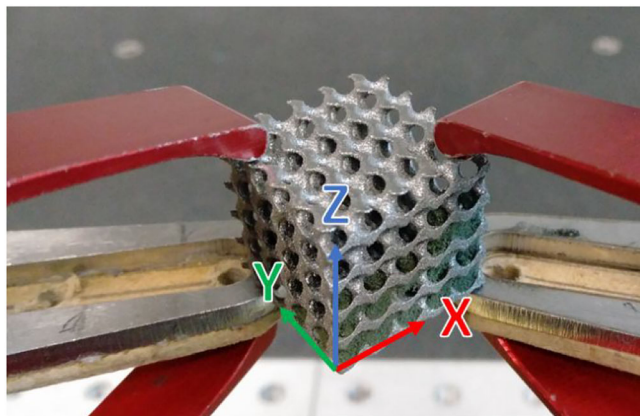


FIGURE 6 Reference system of the aligned gyroid part

system, and the same probing vectors. Using the same virtual probing points in a CT measurement is dependent on a similar alignment of the scan data.

The adopted alignment in this case was a datum based alignment with three ISO conform datum planes, fitted on three orthogonal sides of the cubic lattice sample, using Chebyshev polynomials and selected orthogonal to each other. Even to derive these planes, it is theoretically necessary to virtually probe exactly the same point for the fitting of these planes. If not, the alignment is different and the results get less comparable. Using areas that are not ambiguous, like subtractive machined, almost perfect planes would make this step easier but is not practical for general additively manufactured components.

In our case, the approach of the typical automotive reference point system (RPS) alignment was used. When aligning very similar to the CMM as a first iteration, this gives the opportunity to probe points that are very close to the CMM points but not identical. After using the derived points to fit the datum planes and do an alignment, the position of the measurement data in the software coordinate system gets more comparable, yet not perfect. After two or three iterations, the transformation between the different alignment systems becomes smaller than the expected measurement error. This effort is absolutely necessary to make sure that the alignment in two different software packages, with metrology data coming from two different technologies, arriving in two different mathematical descriptions in a different orientation, gets comparable.

Using the similar orientation, it is possible to import the measurement points and probing vectors for fitting the geometry elements; see Figure 7.

To derive the planes, a Gauss fit was used without filtering. Also, the same type of distance was calculated between the corresponding planes. Here as well, differences from a variety of possible methods to calculate the distance between two planes could occur, which would be minimum or maximum distance, distance in XYZ rather than just in one coordinate direction, or, like in our case, measuring the axis-distance between centroids of the two planes.

3 | RESULTS AND DISCUSSION

The strut-based lattice measurement results for CMM and CT using different measurement approaches is summarized in Table 1 and Figure 8. The distances between the planes in X, Y and Z directions are presented (Dist-plane) as well as the distance between the best-fit cylinders (Dist-cyl) in the middle of each plane. The distances between the *mid-points* of the cylinders are used, making these distances smaller than the surface plane distances. The best-fit cylinder distances measured in CT data is shown in Figure 9.

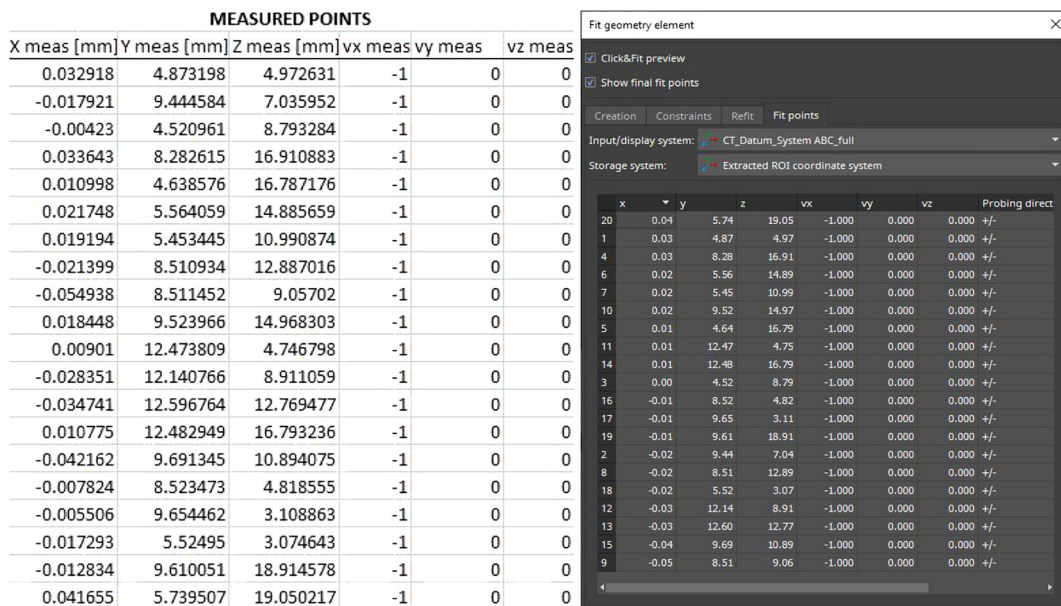


FIGURE 7 (left) Coordinate measurement machine (CMM) probed points in Excel, (right) imported points to VG Metrology, identical position to CMM, virtually probed in VG Metrology

TABLE 1 Comparison of the CAD dimensions of the strut-design sample with the results of CMM and CT measurements (aligned to CMM coordinate system)

Strut sample	Dist-plane X (mm)	Dist-plane Y (mm)	Dist-plane Z (mm)	Dist-cyl X (mm)	Dist-cyl Y (mm)	Dist-cyl Z (mm)
CAD	20.883	20.889	20.885	19.950	19.950	19.940
CMM	21.150	21.115	20.180	20.000	19.968	19.672
CT	21.057	21.045	20.182	20.132	19.993	19.725

Abbreviations: CAD, computer-aided design; CMM, coordinate measurement machine; CT, computed tomography.

FIGURE 8 Bar charts of the computer-aided design (CAD), coordinate measurement machine (CMM) and computed tomography (CT) dimensions of strut-based lattice

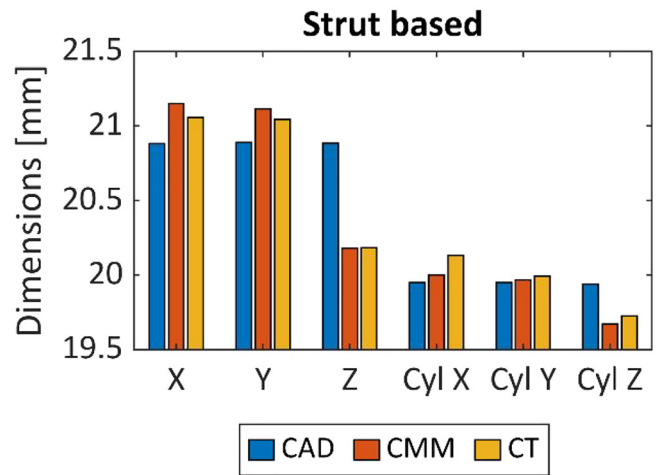
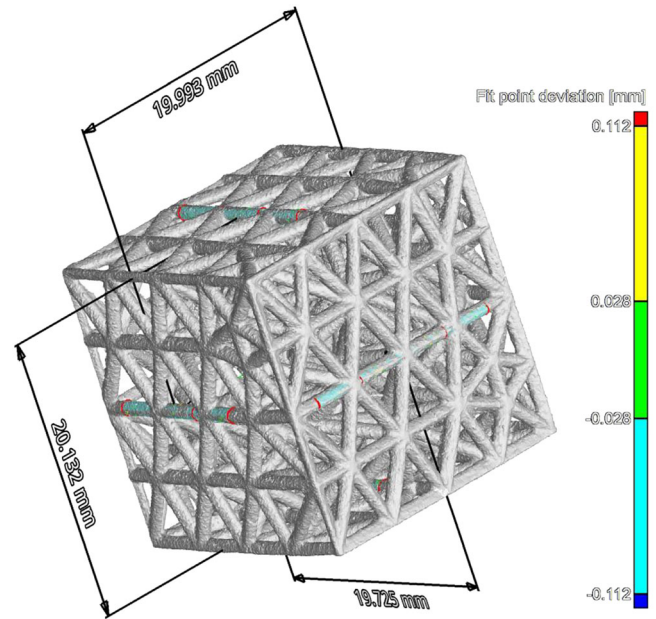


FIGURE 9 Visualization of the measurement of best-fit cylinders and distances between them



The analysis of the above data reveals that dimensions derived by both CT and CMM measurements are higher than CAD dimensions in X and Y direction. The dimensional accuracy of L-PBF manufacturing depends on many factors, including the calibration of scanning mirrors, the laser power and scan speed, scanning strategy, contour offset, amongst others. Such processing parameters affect the track size and location, which affects the eventual dimensions of the part. In addition, the roughness varies with different inclination angles relative to the build direction. The higher dimensions in X and Y directions in particular might be attributed to an excessive local heating, which might have caused partial melting and attachment of powder particles, as observed in Dallago et al.³⁹

On the contrary, the trend is different for the Z direction. The lower dimension derived from measurements in comparison to CAD is explained by the removal of samples from the building plate, as the removal was not done accurately and removed too much material.

Comparing the CMM and CT, dimensions are slightly higher in CMM than CT, when comparing the measured distance between planes. There are various possible reasons for these differences: surfaces are not actually flat, and CMM measurement is influenced by the diameter of the tip sphere (1 mm), whereas CT allows higher resolution inspecting curved surfaces. Consequently, when the tip sphere approaches the nominal point, the contact might have occurred on the higher point of the convex strut section in the area of approaching direction due to the surface roughness. Therefore, CMM evaluates the maximum material condition of the dimension derived by the distance between planes.

An opposite trend is observed comparing CMM and CT results derived by the distance between cylinder axes. In this case, CT dimensions are higher than CMM data, but the reason might be the same explained above, as shown in Figure 10. Two strut sections are schematized by the nominal circular section (thin black line), whereas the actual profile corresponds to the irregular bold black line. Figure 10 shows that the CMM tip sphere has the same nominal dimension of the nominal strut section. Therefore, when the CMM tip sphere would touch the nominal blue points selected on the CAD model, the real measured points lie on the first protuberance, as schematized by the red dots. On the contrary, CT should be able to inspect the actual points (green dots, overlapped to the blue nominal points) on the actual profile. The cylinder reconstructed by CMM measured points is consequently larger than the cylinder reconstructed by CT data, because CMM can only acquire points on the convex segment of the actual profile, whereas CT could also inspect points on the concave profile. Therefore, the results of the CMM measurement are affected by the size of the tip sphere and the inhomogeneous surface roughness which might determine an overestimation of the diameter size, as confirmed by Table 2, and a lower distance between cylinder axes, as observed in Figure 8 and Table 1. Better agreement between CMM and CT data is observed along the Z distance, likely due to the better surface quality of the bottom surface after sample removal by the cutting operation.

The gyroid lattice structure results are reported in Table 3 and Figure 11. As observed on the strut-based lattice, both CT and CMM measurements are higher than CAD dimensions in X and Y directions, whereas they are lower in the Z direction for the same reasons described above.

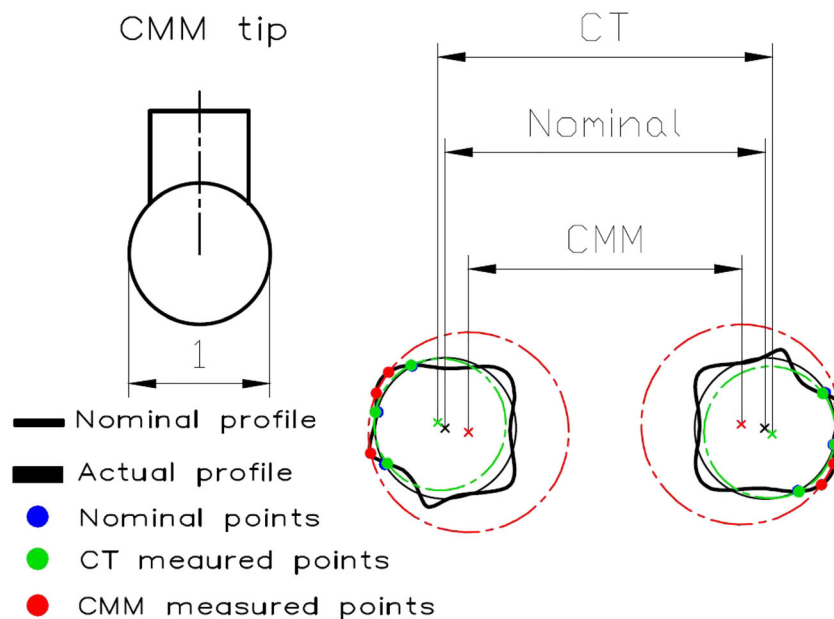


FIGURE 10 Proposed explanation for the different results of coordinate measurement machine (CMM) and computed tomography (CT) results as cylinder diameters and axes distance

TABLE 2 Diameter of the struts measured by CT and CMM—struts are identified by a conventional name and by the coordinates of the centroid, according to the reference system sketched in Figure 3

Cylinder reference name (centroid coordinates)	Diameter (mm)	
	CT	CMM
Cyl B (X = 0; Y = 9.975; Z = 9.97)	1.018	1.145
Cyl B2 (X = 19.95; Y = 19.95; Z = 9.97)	1.178	1.048
Cyl C (X = 9.975; Y = 0; Z = 9.97)	0.994	1.157
Cyl C2 (X = 19.95; Y = 19.95; Z = 9.97)	1.004	1.089
Cyl A2 (X = 9.975; Y = 9.975; Z = 0)	0.778	0.946

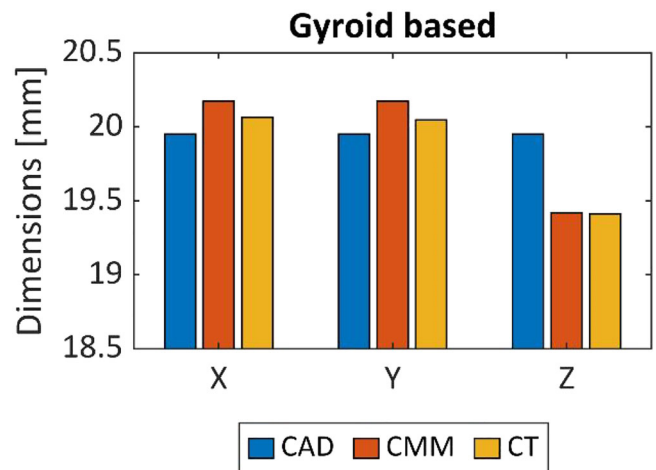
Abbreviations: CMM, coordinate measurement machine; CT, computed tomography.

TABLE 3 Comparison of the CAD dimensions of the gyroid sample with the results of CMM and CT measurements

Gyroid sample	Plane X (mm)	Plane Y (mm)	Plane Z (mm)
CAD	19.950	19.950	19.950
CMM	20.175	20.175	19.420
CT (cmm)	20.064	20.048	19.412
CT (Pts)	20.012	20.012	19.385

Abbreviations: CAD, computer-aided design; CMM, coordinate measurement machine; CT, computed tomography.

FIGURE 11 Bar chart of the computer-aided design (CAD) dimensions and coordinate measurement machine (CMM) and computed tomography (CT) measurements of gyroid-based lattice



High agreement between CMM and CT is highlighted in the Z direction, whereas CMM dimensions are higher than CT dimensions on X and Y directions, when comparing the measured distance between planes, as also observed in the strut-based sample. The tip diameter and the surface roughness might again have played a significant role, as previously described. The dimensions are illustrated in Figure 12.

The above results highlight the most important factors to consider in a dual measurement approach—ensuring coordinate systems are selected the same and ideally that the same points are probed in both CMM and CT. Differences in measurements could be explained, and the potential to use this approach is clearly demonstrated. Recent work describing different approaches to determining measurement uncertainties in CT dimensional measurements are presented in Villarraga-Gómez et al.⁴⁰

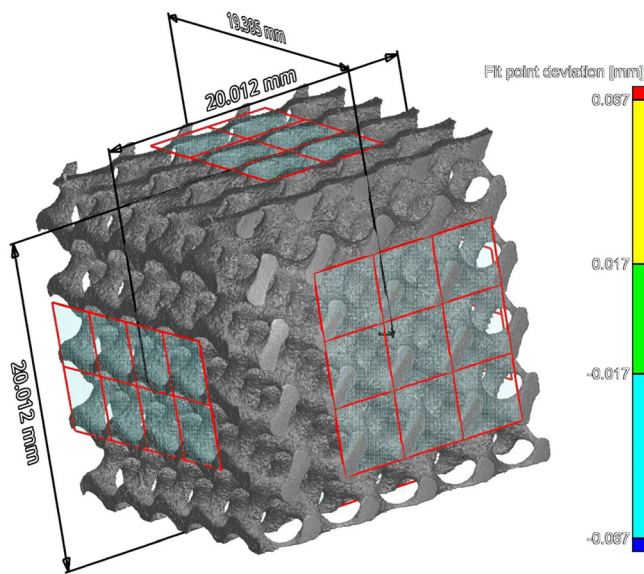


FIGURE 12 Computed tomography (CT) visualization of measured dimensions for gyroid lattice sample

4 | CONCLUSIONS

We have demonstrated a combined workflow for CMM and CT measurements of lattice structures. The most important challenges with this approach to dimensional metrology of lattice structures were highlighted. On the one hand, CMM is traceable and highly accurate, but fit-points might be affected by the probe size, the surface roughness of additively manufactured parts, and the access is limited, making selection of good fit-points challenging even on the surface (as shown for the cylinders for example). On the other hand, CT provides a wealth of possible information including much more surface data on all surfaces, internal pores inside struts and other flaw types internal to the structure. However, in the case of measurements by CT, traceability is in question if a dedicated metrology CT system is not used. Despite these issues, the reported results for CT and CMM are within a maximum of 150 μm of each other in this case study despite the above-mentioned issues, becoming much better for the Z-direction with one surface cut (no as-built roughness)—the largest measured difference was 53 μm in this case. This means that the bulk of the differences lie in the surface probing differences and point definitions due to roughness. By careful selection alignment axes, probing the same points and selecting the same measurement strategy, further improved correlation can be obtained. In the case of required metrology traceability for dimensional measurements inside lattice structures, the selected CMM surface measurements could be used for a virtual calibration of the CT dataset, to correct these discrepancies, and allow internal measurements to be made using CT data were needed. The work has thus highlighted the importance of measurement strategies and approaches for both CMM and CT of complex lattice structures.

DATA AVAILABILITY STATEMENT

Data are available on request.

ORCID

Anton du Plessis  <https://orcid.org/0000-0002-4370-8661>

Matteo Benedetti  <https://orcid.org/0000-0001-9158-2429>

REFERENCES

- Gibson I., Rosen D., Stucker B., *Additive Manufacturing Technologies: 3D Printing, Rapid Prototyping, and Direct Digital Manufacturing*, second edition, 2015. <https://doi.org/10.1007/978-1-4939-2113-3>
- Leary M. *Design for additive manufacturing*, 2019.
- du Plessis A, Broeckhoven C, Yadroitsava I, et al. Beautiful and functional: A review of biomimetic design in additive manufacturing. *Addit. Manuf.* 2019;27:408-427. <https://doi.org/10.1016/j.addma.2019.03.033>
- Yadroitsev I, Yadroitsava I, Du Plessis A, MacDonald E, eds., *Fundamentals of Laser Powder Bed Fusion of Metals*, 1st Edition, Elsevier, 2021. <https://www.elsevier.com/books/fundamentals-of-laser-powder-bed-fusion-of-metals/yadroitsev/978-0-12-824090-8>

5. Debroy T, Wei HL, Zuback JS, et al. Additive manufacturing of metallic components—process, structure and properties. *Prog. Mater. Sci.* 2018;92:112-224. <https://doi.org/10.1016/j.pmatsci.2017.10.001>
6. DebRoy T, Mukherjee T, Milewski JO, et al. Scientific, technological and economic issues in metal printing and their solutions. *Nat. Mater.* 2019;1026-1032. <https://doi.org/10.1038/s41563-019-0408-2>
7. Ashby MF. The properties of foams and lattices. *Philos. Trans. R. Soc. A Math. Phys. Eng. Sci.* 2006;364:15-30. <https://doi.org/10.1098/rsta.2005.1678>
8. Gibson LJ, Ashby MF. *Cellular Solids: Structure and Properties*. second ed. ; 2014 <https://doi.org/10.1017/CBO9781139878326>
9. Maconachie T, Leary M, Lozanovski B, et al. SLM lattice structures: Properties, performance, applications and challenges. *Mater Des.* 2019;183:1-8, 108137. <https://doi.org/10.1016/j.matdes.2019.108137>
10. Yadroitsava I, du Plessis A., Yadroitsev I., Bone regeneration on implants of titanium alloys produced by laser powder bed fusion: a review, 2019. <https://doi.org/10.1016/B978-0-12-815820-3.00016-2>
11. Arabnejad S, Johnston B, Tanzer M, Pasini D. Fully porous 3D printed titanium femoral stem to reduce stress-shielding following total hip arthroplasty. *J Orthop Res.* 2017;35:1774-1783. <https://doi.org/10.1002/jor.23445>
12. Zadpoor AA. Mechanical performance of additively manufactured meta-biomaterials. *Acta Biomater.* 2019;85:41-59. <https://doi.org/10.1016/J.ACTBIO.2018.12.038>
13. Bhate D, Penick C, Ferry L, et al. Classification and selection of cellular materials in mechanical design: engineering and biomimetic approaches. *Designs.* 2019;3:1-31. <https://doi.org/10.3390/designs3010019>
14. Murr LE. Open-cellular metal implant design and fabrication for biomechanical compatibility with bone using electron beam melting. *J Mech Behav Biomed Mater.* 2017;76:164-177. <https://doi.org/10.1016/J.JMBBM.2017.02.019>
15. Van Bael S, Kerckhofs G, Moesen M, Pyka G, Schrooten J, Kruth JP. Micro-CT-based improvement of geometrical and mechanical controllability of selective laser melted Ti6Al4V porous structures. *Mater Sci Eng A.* 2011;528:7423-7431. <https://doi.org/10.1016/J.MSEA.2011.06.045>
16. Maleki E, Bagherifard S, Bandini M, Guagliano M. Surface post-treatments for metal additive manufacturing: progress, challenges, and opportunities. *Addit Manuf.* 2020;1-22, 101619. <https://doi.org/10.1016/j.addma.2020.101619>
17. Lee P.H., Chung H., Lee S.W., Yoo J., Ko J., Review: dimensional accuracy in additive manufacturing processes, in: ASME 2014 Int. Manuf. Sci. Eng. Conf. MSEC 2014 Collocated with JSME 2014 Int. Conf. Mater. Process. 42nd North Am. Manuf. Res. Conf., Web Portal ASME (American Society of Mechanical Engineers), 2014. <https://doi.org/10.1115/MSEC2014-4037>
18. Fotovvati B, Asadi E. Size effects on geometrical accuracy for additive manufacturing of Ti-6Al-4V ELI parts. *Int J Adv Manuf Technol.* 2019;104:2951-2959. <https://doi.org/10.1007/s00170-019-04184-1>
19. Savio E, De Chiffre L, Carmignato S, Meinertz J. Economic benefits of metrology in manufacturing. *CIRP Ann - Manuf Technol.* 2016;65:495-498. <https://doi.org/10.1016/j.cirp.2016.04.020>
20. Villarraga-Gómez H, Herazo EL, Smith ST. Progression of X-ray computed tomography from medical imaging to current status in dimensional metrology. *Precis Eng.* 2019;544-569. <https://doi.org/10.1016/J.PRECISIONENG.2019.06.007>
21. Kruth JP, Bartscher M, Carmignato S, Schmitt R, De Chiffre L, Weckenmann A. Computed tomography for dimensional metrology. *CIRP Ann - Manuf Technol.* 2011;60:821-842. <https://doi.org/10.1016/j.cirp.2011.05.006>
22. Ferrucci M, Leach RK, Giusca C, Carmignato S, Dewulf W. Towards geometrical calibration of X-ray computed tomography systems—a review. *Meas Sci Technol.* 2015;26:1-30. <https://doi.org/10.1088/0957-0233/26/9/092003>
23. Buratti A., Bredemann J., Pavan M., Schmitt R., Carmignato S., Applications of CT for dimensional metrology, in: *Ind. X-Ray Comput. Tomogr.*, Springer International Publishing, 2017: pp. 333–369. https://doi.org/10.1007/978-3-319-59573-3_9
24. Villarraga-Gómez H, Lee CB, Smith ST. Dimensional metrology with X-ray CT: a comparison with CMM measurements on internal features and compliant structures. *Precis Eng.* 2018;51:291-307. <https://doi.org/10.1016/j.precisioneng.2017.08.021>
25. du Plessis A., Yadroitsev I., Yadroitsava I., Le Roux S.G., X-ray microcomputed tomography in additive manufacturing: a review of the current technology and applications, *3D Print. Addit. Manuf.* 5 (2018) 3dp.2018.0060. <https://doi.org/10.1089/3dp.2018.0060>
26. du Plessis A, Yadroitsava I, Yadroitsev I. Effects of defects on mechanical properties in metal additive manufacturing: a review focusing on X-ray tomography insights. *Mater Des.* 2020;187:1-19. <https://doi.org/10.1016/j.matdes.2019.108385>
27. Dallago M, Winiarski B, Zanini F, Carmignato S, Benedetti M. On the effect of geometrical imperfections and defects on the fatigue strength of cellular lattice structures additively manufactured via Selective Laser Melting. *Int J Fatigue.* 2019;124:348-360. <https://doi.org/10.1016/j.ijfatigue.2019.03.019>
28. Boniotti L, Beretta S, Patriarca L, Rigoni L, Foletti S. Experimental and numerical investigation on compressive fatigue strength of lattice structures of AlSi7Mg manufactured by SLM. *Int J Fatigue.* 2019;128:1-14, 105181. <https://doi.org/10.1016/j.ijfatigue.2019.06.041>
29. Liu L, Kamm P, García-Moreno F, Banhart J, Pasini D. Elastic and failure response of imperfect three-dimensional metallic lattices: the role of geometric defects induced by Selective Laser Melting. *J Mech Phys Solids.* 2017;107:160-184. <https://doi.org/10.1016/j.jmps.2017.07.003>
30. Liu YJ, Wang HL, Li SJ, et al. Compressive and fatigue behavior of beta-type titanium porous structures fabricated by electron beam melting. *Acta Mater.* 2017;126:58-66. <https://doi.org/10.1016/j.actamat.2016.12.052>
31. Bauza M.B., Moylan S.P., Panas R.M., Burke S.C., Martz H.E., Taylor J.S., Alexander P., Knebel R.H., Bhogaraju R., O'connell M.T., Smokovitz J.D., Study of accuracy of parts produced using additive manufacturing, in: ASPE Spring Top. Meet. Dimens. Accuracy Surf. Finish Addit. Manuf., 2014: pp. 86–91. https://tsapps.nist.gov/publication/get_pdf.cfm?pub_id=915785 (accessed November 20, 2020).

32. Carmignato S, De Chiffre L, Bosse H, Leach RK, Balsamo A, Estler WT. Dimensional artefacts to achieve metrological traceability in advanced manufacturing. *CIRP Ann.* 2020;69:693-716. <https://doi.org/10.1016/j.cirp.2020.05.009>
33. Rivas Santos VM, Thompson A, Sims-Waterhouse D, Maskery I, Woolliams P, Leach R. Design and characterisation of an additive manufacturing benchmarking artefact following a design-for-metrology approach. *Addit Manuf.* 2020;32:1-8, 100964. <https://doi.org/10.1016/j.addma.2019.100964>
34. Zanini F, Sorgato M, Savio E, Carmignato S. Uncertainty of CT dimensional measurements performed on metal additively manufactured lattice structures, 10th Conf. *Ind Comput Tomogr.* 2020;1-6. www.ict-conference.com/2020
35. du Plessis A, Tshibalanganda M, le Roux SG. Not all scans are equal: X-ray tomography image quality evaluation. *Mater Today Commun.* 2020;22:1-10, 100792. <https://doi.org/10.1016/j.mtcomm.2019.100792>
36. du Plessis A, Razavi SMJ, Berto F. The effects of microporosity in struts of gyroid lattice structures produced by laser powder bed fusion. *Mater Des.* 2020;194:1-10, 108899. <https://doi.org/10.1016/j.matdes.2020.108899>
37. ISO - ISO 10360-2: 2009—Geometrical product specifications (GPS)—Acceptance and reverification tests for coordinate measuring machines (CMM)—Part 2: CMMs used for measuring linear dimensions, (n.d.). <https://www.iso.org/standard/40954.html> (accessed November 20, 2020).
38. du Plessis A, le Roux SG, Tshibalanganda M. Advancing X-ray micro computed tomography in Africa: Going far, together. *Sci African.* 2019;3:1-13, e00061. <https://doi.org/10.1016/j.sciaf.2019.e00061>
39. Dallago M, Raghavendra S, Luchin V, Zappini G, Pasini D, Benedetti M. Geometric assessment of lattice materials built via Selective Laser Melting. *Mater Today Proc.* 2019;7:353-361. <https://doi.org/10.1016/j.matpr.2018.11.096>
40. Villarraga-Gómez H, Thousand JD, Smith ST. Empirical approaches to uncertainty analysis of X-ray computed tomography measurements: a review with examples. *Precis Eng.* 2020;64:249-268. <https://doi.org/10.1016/j.precisioneng.2020.03.004>

How to cite this article: du Plessis A, Schwaderer G, Cristofolini I, Zago M, Benedetti M. Dimensional metrology of additively manufactured lattice structures by combined tactile probe and X-ray tomography. *Mat Design Process Comm.* 2021;1–12. <https://doi.org/10.1002/mdp2.216>